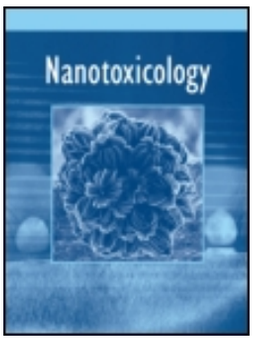

Nanotoxicology

ISSN: 1743-5390 (Print) 1743-5404 (Online) Journal homepage: http://www.tandfonline.com/loi/inan20

Inflammatory response of mice following inhalation exposure to iron and copper nanoparticles

John M. Pettibone, Andrea Adamcakova-Dodd, Peter S. Thorne, Patrick T. O'Shaughnessy, Jamie A. Weydert & Vicki H. Grassian

To cite this article: John M. Pettibone, Andrea Adamcakova-Dodd, Peter S. Thorne, Patrick T. O'Shaughnessy, Jamie A. Weydert & Vicki H. Grassian (2008) Inflammatory response of mice following inhalation exposure to iron and copper nanoparticles, Nanotoxicology, 2:4, 189-204, DOI: 10.1080/17435390802398291

To link to this article: http://dx.doi.org/10.1080/17435390802398291

Published online: 10 Jul 2009.

Nanotoxicology, December 2008; 2(4): 189–204

informa
healthcare

Inflammatory response of mice following inhalation exposure to iron and copper nanoparticles

JOHN M. PETTIBONE[1], ANDREA ADAMCAKOVA-DODD[2], PETER S. THORNE[2], PATRICK T. O'SHAUGHNESSY[2], JAMIE A. WEYDERT[3], & VICKI H. GRASSIAN[1,2,4]

[1]*Chemical and Biochemical Engineering;* [2]*Occupational and Environmental Health;* [3]*Pathology &* [4]*Chemistry, University of Iowa, Iowa City, Iowa, USA*

(Received 9 May 2008; accepted 8 August 2008)

Abstract
We examined pulmonary inflammatory responses of mice following whole-body inhalation exposure to copper and iron nanoparticles in acute and sub-acute studies. Concentrations for sub-acute copper and iron exposures were 3.6 mg m^{-3}. No significant pathology was found following acute exposure. Immediately following sub-acute exposure, both iron- and copper-exposed mice showed increased inflammation compared to sentinels. Copper nanoparticle-exposed mice had significantly higher lavage cytokines as well as perivasculitis and alveolitis. Three weeks post-exposure, all inflammatory markers decreased for iron nanoparticle-exposed mice, however, some remained elevated for copper-exposed mice. At biologically relevant pHs, *in vitro* studies showed that copper nanoparticles displayed a greater propensity for dissolution compared to iron. We conclude that the presence of dissolved ions, the concomitant formation of smaller nanoparticles and the absence of particles in stained lung sections immediately postexposure (inferring either translocation or more dispersed aerosol distribution) contributed to the increased inflammation observed in copper nanoparticle-exposed mice.

Keywords: *Aerosol, inhalation, murine models, dissolution, copper, iron, nanoparticles, agglomerates*

Introduction

Transition metal nanomaterials are finding more applications in a number of industrial processes and consumer products. Iron nanoparticles are used in medical imaging (Babes et al. 1999), media storage (Chen and Gao 2004), and in fluid applications as well as for environmental remediation (Zhang 2003). Copper nanoparticles are used as sensors, catalysts and as additives in lubricant oils (Liu et al. 2004). Human exposure to these transition metal nanomaterials may occur in the manufacturing process as well as during handling, transport and use. Thus, investigations are needed to determine if there are harmful health effects associated with exposure.

Previous studies have shown that inhalation is the most probable exposure route for metal nanoparticles in a systemic dose (Osier and Oberdörster 1997; Driscoll et al. 2000). Currently, there is no direct correlation of biological markers for response between *in vivo* and *in vitro* studies due to the complexity of dose delivery, single vs. cocultures, endpoint evaluations as well as other factors of cellular interaction with different biological media (Seagrave et al. 2005; Sayes et al. 2007); therefore, *in vivo* studies are currently more relevant for risk assessment. As such, the study described here is designed to compare toxicity of two commonly used commercially available, transition metal nanoparticles in inhalation studies.

It is becoming increasingly clear that an integrated approach which includes both inhalation toxicology studies and full characterization of the nanomaterials is necessary for understanding inflammatory responses as they relate to the physicochemical principles of nanoparticles. The importance of characterizing nanoparticles in health-related studies has been recommended in a number of workshop reports (Oberdörster et al. 2005; Balbus et al. 2007; Powers et al. 2007; Warheit et al. 2007) and has been used in our studies on titanium dioxide nanoparticles (Grassian et al. 2007a,b). In addition, full characterization of manufactured nanomaterials, even when there is some physical and chemical characterization provided by the manufacturer, is necessary because of batch-to-batch variation, difficulties associated with quality control for the

Correspondence: Vicki H. Grassian, Department of Chemistry, University of Iowa, Iowa City IA 52242, USA. Tel: +1 310 335 1392. Fax: +1 319 335 1270. E-mail: vicki-grassian@uiowa.edu

ISSN 1743-5390 print/ISSN 1743-5404 online
DOI: 10.1080/17435390802398291

production of large quantities of some nanomaterials and difficulties with the ability to do rapid and routine nanoparticle characterization.

Another important physicochemical factor in the toxicity of the nanoparticles that must be determined is the degree of nanoparticle aggregation or agglomeration present in airborne aerosols. According to ASTM International (ASTM International Committee E56 on Nanotechnology, 2006), particle agglomerates are defined as a group of particles held together by relatively weak forces, e.g., van der Waals or capillary, that may break apart into smaller particles, whereas particle aggregates are defined as a group of particles in which the various individual components are strongly bonded together, e.g., fused, sintered or chemically bonded. Agglomerates have a higher potential to disperse into smaller primary particles. Deagglomeration can occur after deposition in the airway surface liquid. Whether nanoparticles deagglomerate or remain as larger agglomerates will be an important factor in how nanoparticles translocate or undergo clearance. If nanoparticles cannot break apart into primary particles once deposited into the body, an important dose metric may be the projected surface area of the nanoparticle agglomerate (Moss and Wong 2007). Other properties such as nanoparticle dissolution may also be affected by agglomeration (Midander et al. 2007). Therefore, characterizing both primary particle and agglomerate/aggregation size is important as it can affect deposition, clearance and cellular responses in the body (Zhang et al. 1999; Gilbert et al. 2004; Kakkar et al. 2004; Grassian et al. 2007b).

In the current study, an integrated approach was used to examine the pulmonary inflammatory responses of two different types of inhaled transition metal nanoparticles in mice. In particular, mice were exposed to copper and iron nanoparticles with a manufacturer's reported average particle size of 25 nm and, according to manufacturer's specifications, these nanoparticles have been partially passivated with oxygen to form an oxide surface coating. A relative comparison of nanoparticle toxicity was conducted using acute and sub-acute exposures in a whole body chamber. Bronchoalveolar lavage (BAL) fluid cellularity, total protein, lactate dehydrogenase activity and cytokines as well as lung histopathology were evaluated to assess responses. In addition, these nanoparticles were fully characterized using bulk and surface techniques to better understand their physicochemical properties. Dissolution studies of nanoparticles in two artificial biological fluids were conducted to better understand pulmonary effects of metal nanoparticles and how they are processed once they are inhaled and retained in the lungs.

Methods

Sources of manufactured nanoparticles

Copper and iron nanoparticles with a manufacturer's stated average particle size of 25 nm were purchased from Nanostructured and Amorphous Materials, Inc (Houston, TX, USA) as powder samples. The nanoparticles were used as received from the manufacturer without modification.

Particle characterization

The bulk crystalline phases of the nanoparticles were determined using powder x-ray diffraction (XRD) measurements (Bruker D-5000 q – q diffractometer with Kevex-sensitive detector, (Madison, WI, USA). XRD can determine the crystalline phases present by measuring the X-ray reflections as a function of scattering angle (Atkins and De Paula 2002). Transmission electron microscopy (TEM) was used to measure the primary particle size of 50 random nanoparticles and compare the average to manufacturer's specifications. TEM was also used to measure agglomerate sizes of the metal nanoparticle aerosols generated in the inhalation chamber.

Surface properties were examined by measuring surface area and characterizing the surface composition. Surface area measurements were made on an automated multipoint BET surface area apparatus (Quantachrome Nova 4200e, Boynton Beach, FL, USA) using nitrogen as the adsorbent. X-ray photoelectron spectroscopy (XPS) was used to probe the surface chemical composition characteristics of the metal nanoparticles (custom-designed Ultra-Axis XPS system from Kratos, Manchester, UK).

Dissolution studies

Acid dissolution studies were conducted to measure the propensity of nanoparticle dissolution at different and physiologically relevant pH values (Stopford et al. 2003; Midander et al. 2006, 2007). The solubility of metal nanoparticles and their interaction with the cells has been shown to be an important factor in cellular response (Knaapen et al. 2002; Borm et al. 2006; Brunner et al. 2006; Midander et al. 2007). The standard redox potentials in oxygenated water for bulk iron and copper to the ferrous and cupric ions were calculated to be 0.848 and 0.059 eV, respectively, inferring that iron would more readily dissociate into ions than copper. However, dissolution is often a kinetically and not thermodynamically controlled process. Other considerations such as the solubility of the surface oxide and dissolution in biological fluids where ligand-promoted dissolution can occur may be the most

important factors in controlling nanoparticle dissolution.

Relevant dissolution studies were conducted in two different types of artificial fluids, artificial lysomal fluid (ALF) and Gamble's solution. The ALF fluid simulates the phagolysosomal composition and pH of alveolar and interstitial macrophages (Stopford et al. 2003; Midander et al. 2007) and the Gamble's solution is used to mimic the interstitial fluid in the lungs (Moss 1979). The ALF solution has the largest percent by weight of citric acid for the purpose of imitating protein binding along with other potential ligands such as acetate to represent organic acids present. The ALF solution has a pH of 4.5–5. Gamble's solution also contains similar constituents but the citrate concentration is much lower and is buffered at pH 7.2–7.4 with $NaHCO_3$. All solutions were prepared in glassware that was acid cleaned with 1 M HCl (Fisher Scientific, reagent grade). Optima water (Fisher Scientific) was used to make all solutions.

Batch reactor studies were conducted on the iron and copper nanoparticles to measure total nanoparticle dissolution in the ALF and Gamble's solutions. These studies were conducted in 7 ml crimp-sealed glass vials and were mixed with a magnetic stir bar. The reactors were filled with 6 ml of the simulated fluid and 5 mg of the metal nanoparticles were added. The vial was immediately sealed and placed into a water bath circulating at 38°C. The water bath was covered with black felt to minimize any light-induced effects and was stirred for 24 h. After this time, solutions were sent through a syringe driven 0.2 μm filter and centrifuged for 20 min at 15,000 rpm (21,000 RCF). Several different procedures were used for the filtering process to make certain that the measurements of dissolved metal included only dissolved ions and no nanoparticles were present in solution. These included measuring samples after filtration, after centrifugation and the filtered solutions were also ultracentrifuged for 1 h at 70,000 rpm. The filtered solutions were analyzed using a Varian inductively coupled plasma (ICP) equipped with optical emissions spectrometer (OES) detector to quantify the total amount of iron or copper in the filtered solutions.

In some cases, following these 24-h dissolution studies, kinetic measurements for metal nanoparticle dissolution were performed at 38°C in a 100 ml glass reaction vessel equipped with a water jacket to control temperature. The experiments were run in a 50 ml water suspension that contained 25 mg of nanoparticles while mixed with a magnetic stir bar. The nanoparticles were added when the desired temperature had been reached. The first 1 ml sample was taken immediately after the pH had been adjusted and then every 15 min for 1.5 h. The dissolution experiments went for a total time of 36 h. The pH of the system was adjusted with HCl as needed during the reaction to maintain constant pH.

Animals

We purchased 6-week-old C57Bl/6 male mice from The Jackson Laboratory (Bar Harbor, ME, USA). Animals were held in quarantine for 12 days, prior to the start of an experiment, in an on-site, AAALAC-accredited vivarium in polypropylene, fiber-covered cages in HEPA-filtered Thoren caging units (Hazelton, PA, USA). They were supplied with food (sterile Teklad 5% stock diet, Harlan, Madison, WI) and water *ad libidum* and maintained on a 12-h light-dark cycle. The average animal weight at the time of necropsy in acute exposures was 21.4 g. Animals exposed sub-acutely and necropsied at 0 wk post exposure or 3 weeks post exposure had an average weight of 22.3 g and 25.1 g, respectively. Animal protocols were approved by the Institutional Animal Care and Use Committee and complied with the NIH Guide for the Care and Use of Laboratory Animals.

Exposure chamber, aerosol generation and aerosol characterization

The inhalation exposure system was used, as previously described (Grassian et al. 2007a,b). Briefly, mice were placed within sectioned, open-wire cages that were positioned in a whole-body 65-l custom-fabricated aluminum exposure chamber (O'Shaughnessy et al. 2003). The chamber was operated with a flow rate of 25 l min^{-1} provided by a vacuum pump and measured with a calibrated flowmeter.

Nanoparticles were suspended in ultra-pure water (Milli-Q® Academic A-10, Millipore Corp., Billerica, MA, USA) and ultra-sonicated with a high frequency probe (model 550, Fisher Scientific, Pittsburgh, PA, USA) for at least 10 min. The suspension was then atomized with a Collison nebulizer (BGI Inc., Waltham, MA, USA) and passed through a 110°C brass drying column as well as a 20 mCi ^{63}Ni source to remove any excess charge prior to entering the exposure chamber. Gravimetric concentrations (mg m^{-3}) of particles were measured in the chamber with 47-mm glass microfiber filters (Whatman, Middlesex, UK) in line with exhaust air flow. The temperature in the exposure chamber during the experiments ranged between 20–22°C and relative humidity between 25 and 35%. TEM grids were placed on the top of the cages inside the exposure chamber for analysis of

deposited nanoparticles. The size distribution of the aerosol in the whole-body exposure chamber during inhalation exposures was measured using a scanning mobility particle sizer (SMPS) consisting of a condensation particle counter (Model 3010, TSI Inc., St Paul, MN, USA) and an electrostatic classifier with a 'long' differential mobility analyzer (model 3071, TSI Inc., St Paul, MN) that measured in the range of 7.5–311 nm. Average geometric mean (GM) and geometric standard deviation (GSD) of aerosol sizes in individual exposures were calculated from the SMPS measurements.

Inhalation exposure

We used the same inhalation exposure methods as previously described (Grassian et al. 2007a,b). We report on the details of the experimental design, number of animals per exposure group, resulting exposure concentrations, and an estimate of dose administered in Table I. Animals were exposed to iron or copper nanoparticles acutely (4 h per day) and necropsied within one hour after the exposure or sub-acutely (4 hours per day, 5 days per week for 2 weeks) and necropsied within one hour (0 wk) or 3 weeks post exposure (3 wks). The estimated particle mass dose per mouse was calculated assuming a minute volume of 36 ml (Lai 1991) and total particle deposition fraction of 0.2 (Anjilvel and Asgharian 1995). Sentinel animals served as negative controls. We used an established rat model to estimate particle deposition fraction since there is no available mouse model. Furthermore, mathematical models of particle deposition using experimental data found very small differences between mice and rats for particles under 200 nm (Hsieh et al. 1999). Although the concentrations for copper are relatively high compared to the NIOSH recommended exposure limit for dust, the concentrations were needed for short-term toxicology studies to understand the relative toxicity of one compound to the other and to determine the major outcome variables.

Evaluation of Bronchoalveolar lavage (BAL) fluid

Animals were euthanized with an overdose of halothane and exanguinated through the heart. Lungs were lavaged three times with 1 mL of sterile 0.9% sodium chloride solution (Baxter, Deerfield, IL, USA). Recovered BAL fluid was centrifuged and the cell pellet was used for enumeration of total and differential cell counts. The lavage supernatants were split into aliquots and frozen at -80°C for analysis of total protein, lactate dehydrogenase (LDH) activity and cytokine levels. Total protein was determined using a Bradford protein assay (Bio-Rad Laboratories, Inc., Hercules, CA, USA). Activity of LDH in BAL fluid supernatant was measured spectrophotometrically with a commercially available detection kit (Roche Diagnostics, Penzberg, Germany). The concentrations of 23 cytokines and chemokines were measured in the supernatants of BAL fluids of animals exposed sub-acutely using multiplexed fluorescent bead-based immunoassays (Bio-Rad Laboratories, Inc., Hercules, CA). These included interleukin (IL)-1α, IL-1β, IL-2, IL-3, IL-4, IL-5, IL-6, IL-9, IL-10, IL-12 (p40), IL-12 (p70), IL-13, IL-17, Eotaxin, granulocyte colony-stimulating factor (G-CSF), granulocyte macrophage colony-stimulating factor (GM-CSF), interferon (IFN)-γ, keratinocyte-derived cytokine (KC) (a.k.a. CXCL1), monocytye chemotactic protein (MCP)-1, macrophage inflammatory protein (MIP)-1α, MIP-1β, regulated upon activation, normal T-cell expressed and secreted (RANTES) (a.k.a. CCL5), and tumor necrosis factor (TNF)-α.

Table I. Experimental design of sub-acute inhalation animal studies.

Exposure group	Particle concentration in the chamber, mg m^{-3}	Estimated particle mass/ mouse, μg[b]	Calculated particle surface area, cm^2 [c]	*n*
Acute exposure				
Sentinels	–	–	–	5
Fe	7.62	13.2	2.2	6
Cu	6.23	10.8	1.3	6
Sub-acute exposure				
Sentinels	–	–	–	6
Fe 0 wk[a]	3.55	61.3	10.4	8
Fe 3 wks[a]				8
Sentinels	–			8
Cu 0 wk[a]	3.68	63.6	7.6	8
Cu 3 wks[a]				8

[a]Animals were necropsied 0 week (0 wk) or 3 weeks (3 wks) post exposure; [b]Assuming a minute volume of 36 ml and particle deposition of 0.2; [c]Calculated based on measured BET surface areas.

Lung histopathology

After myocardial exsanguination and recovery of BAL fluid, lungs were perfused with sodium chloride and fixed in 10% formaldehyde-phosphate-buffered saline solution via the canulated trachea. The tissue was subsequently paraffin-embedded, sectioned at 5 μm, and stained with hematoxylin and eosin (H & E) as previously described (Thorne et al. 2006). The tissue sections were qualitatively assessed for histopathologic abnormalities by a pathologist via routine light microscopy. The histologic variables assessed included: abnormalities of the parenchymal architecture (bronchioles, alveoli, pleura, and vasculature); abnormal inflammatory infiltrates; presence or absence of acute lung injury; and presence or absence of fibrosis. We also utilized a semi-quantitative scoring system for inflammatory response that was based on the system used by Hamelin et al. (2006). The lungs were assessed for: (i) extent of inflammation (scored in four levels such as 0 = normal, 1 = minimal increase, 2 = moderate increase, 3 = severe increase and/or necrosis and 4 = architectural distortion due to inflammation); and (ii) type of inflammation (scored as follows: a = acute inflammatory cells, b = chronic inflammatory cells and c = mixed inflammatory cells). Briefly, inflammatory cells can be broadly grouped into cells that participate in the early (acute) stage of inflammation versus those that participate in the latter stages of inflammation (chronic). Broadly stated, the predominant inflammatory cell type of acute inflammation is the neutrophil; the predominant cell of chronic inflammation is the lymphocyte. If both acute and chronic inflammatory cells are present within an inflamed portion of tissue, the term 'mixed inflammation' is utilized.

Determination of metals in lung tissue

Lung tissues from two mice in each acutely exposed group were not lavaged but stored at −80°C immediately after harvesting. Lung tissue was weighed and total amounts of iron or copper in lung tissues were determined. High purity nitric acid (Fisher Optima® grade) was used to digest the tissue at 95–98°C. Digestate was diluted to 20 ml with deionized water and metal analysis was performed using inductively coupled plasma mass spectrometry (ICP/MS), ELAN DRC II (Perkin-Elmer, Waltham, MA, USA). The instrument was fitted with a glass (Meinhard) nebulizer and a quartz cyclonic spray chamber. The plasma was operated at 1100 W with the following gas flow rates (ml min^{-1}): Nebulizer 0.95, auxiliary 1.2, plasma 15.5. Rhodium was used as an internal standard at 10 ug l^{-1}. For iron analysis only, the dynamic reaction cell was purged with argon at 0.6 ml min^{-1} to reduce interferences from ArO^+.

To visualize a distribution of iron or copper nanoparticles in lung tissues, we stained the tissues with Perls Prussian Blue Stain or Rhodanine Stain, respectively. Ferric salts are stained as deep blue and copper deposits are observed as brick red. We freely deposited dry nanoparticles on microslides and fixed them with fetal calf serum using a Shandon Cytospin 4 (Thermo Fisher Scientific, Inc., Waltham, MA, USA) for use as positive controls. Furthermore, to imitate the environment in the respiratory system, we put 2 mg of particles into 3.5 ml of artificial lysosomal fluid (ALF) with pH ~4.5 and placed the vials on the shaker for approximately 4 h and then prepared a microslide the same way as with dry particles.

Statistical analyses

We compared data from animals exposed to iron or copper nanoparticles to controls (sentinels) using a *t*-test for unequal variances (SAS Ver. 9.1, SAS, Inc., Cary, NC, USA). Each set of exposures, had their own controls, as shown in Table I. Comparisons between groups exposed to iron and copper nanoparticles were also conducted. A *p*-value less than 0.05 was considered significant.

Results

Particle characterization

XRD patterns of the iron and copper nanoparticles are shown in Figure 1 along with reference diffraction patterns for each of the metals along with diffraction patterns of common oxides for these metals. For iron nanoparticles, three phases are present in the sample; Fe (metallic iron), Fe_3O_4 (magnetite) and γ-Fe_2O_3 (maghemite). The presence of these oxide phases was expected given these metallic nanoparticles are partially passivated with oxygen as reported in the manufacturer's specifications. X-ray diffraction patterns for other common forms of iron oxide such as α-Fe_2O_3 were also compared but not seen to be present in the iron nanoparticle sample. XRD of the copper nanoparticles also shows the presence of three phases, Cu (metallic copper), Cu_2O (cuprite) and CuO (tenorite) as the reference patterns for these three phases (Downs and Hall-Wallace 2003) match the copper nanoparticle diffraction pattern. A diagram of the nanoparticles containing the three phases is shown in Figure 1 showing a metallic core with an oxide surface coating. The most oxidized phase is present at the surface as determined from surface spectroscopy (*vide infa*).

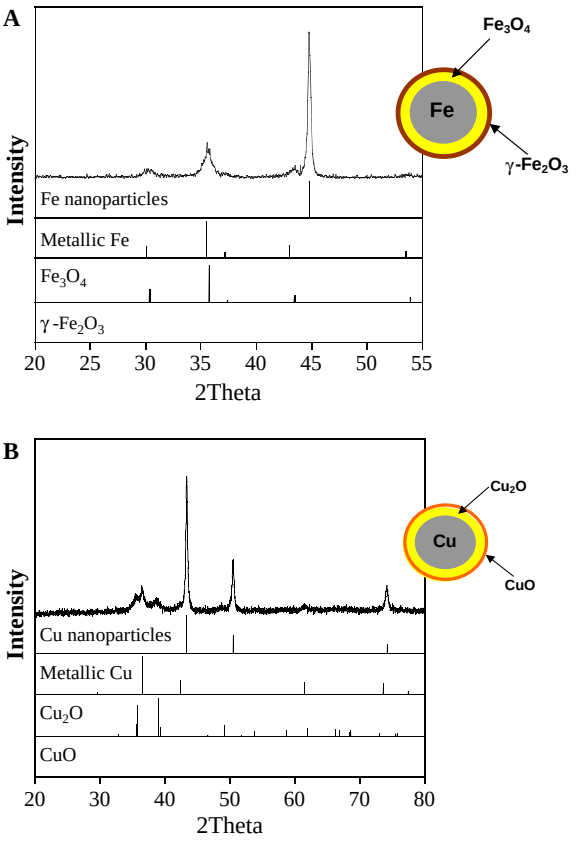

Figure 1. (A) The powder XRD pattern of iron nanoparticles is shown along with reference patterns for metallic Fe, Fe_3O_4 and γ-Fe_2O_3. (B) The powder XRD pattern of copper nanoparticles is shown along with reference patterns for metallic Cu, Cu_2O and CuO. Pictorial representations of iron and copper nanoparticles with these different phases are shown as well. The nanoparticle consists of a metallic core with a gradient of oxidized phases. The most oxidized phase is at the surface (see text for further details).

The particle size and morphology of the iron and copper nanoparticles were examined using TEM (Figure 2). The TEM images are of the nanoparticle agglomerates collected in the whole body chamber during animal exposure. The iron nanoparticle agglomerate is seen in the left image of Figure 2A. Individual iron nanoparticles can be seen in the right for a higher magnified image. The average primary size of the iron nanoparticles was determined to be 25 ± 2 nm from measuring 50 randomly selected nanoparticles that could be easily distinguished from others in an agglomerate. The iron nanoparticles appear in the image on the right to show a core of iron and an oxide coating approximately 3.5 nm in thickness.

Figure 2B shows TEM images of the copper nanoparticles at two different magnifications. These images show that the copper nanoparticles are smaller than the manufacturer's stated average particle size of 25 nm. An average primary particle size of 12 ± 1 nm was measured from over 50 randomly selected nanoparticles. The iron and copper nanoparticles produced an aerosol with a GM near 200 nm and GSDs of 1.3, indicating the production of agglomerates much bigger than the primary particle sizes but with a narrow distribution (Table II).

Surface area measurements for the iron and copper nanoparticles yield a BET surface area of $17 \pm 1\ m^2\ g^{-1}$ and $12 \pm 0.2\ m^2\ g^{-1}$, respectively. Geometric surface areas of the two nanoparticles based on bulk densities of iron and copper metal were calculated to be higher, $35\ m^2\ g^{-1}$ and $60\ m^2\ g^{-1}$, respectively. Surface characterization data for the iron and copper nanoparticles using XPS are shown in Figure 3 for the Fe 2p and Cu 2p regions, respectively. For the iron nanoparticles, reference spectra collected for γ-Fe_2O_3 and Fe_3O_4, the two phases identified in XRD, are also shown. Based on the shape and peak positions, XPS shows that the chemical composition and phase of the surface of the nanoparticles is γ-Fe_2O_3. The TEM and XPS data allows us to surmise that within the nanoparticles there exists an oxygen concentration gradient from the center of the nanoparticle which has no oxygen in the most reduced state (metallic iron, Fe^0) to the surface of the nanoparticle which is the most oxidized state (maghemite, Fe^{3+}) as shown in Figure 1. Under ambient conditions of temperature and relative humidity, oxide surfaces will be truncated with oxygen, surface hydroxyl groups and adsorbed water (Al-Abadleh and Grassian 2003).

The copper nanoparticles show a photoelectron peak with a binding energy of 934.0 eV as well as satellites peaks characteristic of d^9 metals at higher binding energies (Wu et al. 2006). The reference XPS data for CuO is very similar to that of the copper nanoparticles whereas the Cu_2O spectrum is qualitatively and quantitatively very different with an intense peak in the spectrum at 932.8 eV not present in the copper nanoparticle spectrum. These data are consistent with previous studies that oxide copper metal nanoparticle surfaces are Cu(II) oxide, i.e., CuO (Yin et al. 2005).

Surface chemistry – dissolution studies

Dissolution is a surface phenomenon and here we investigated the propensity of iron and copper nanoparticles to dissolve into ions under physiologic conditions. The solutions were designed to represent dissolution in the airway surface liquid or in the macrophage phagolysosome and have considerably different pH values. The ALF solution has a large amount of citric acid simulating the proteins released to dissolve foreign materials. In the ALF solutions,

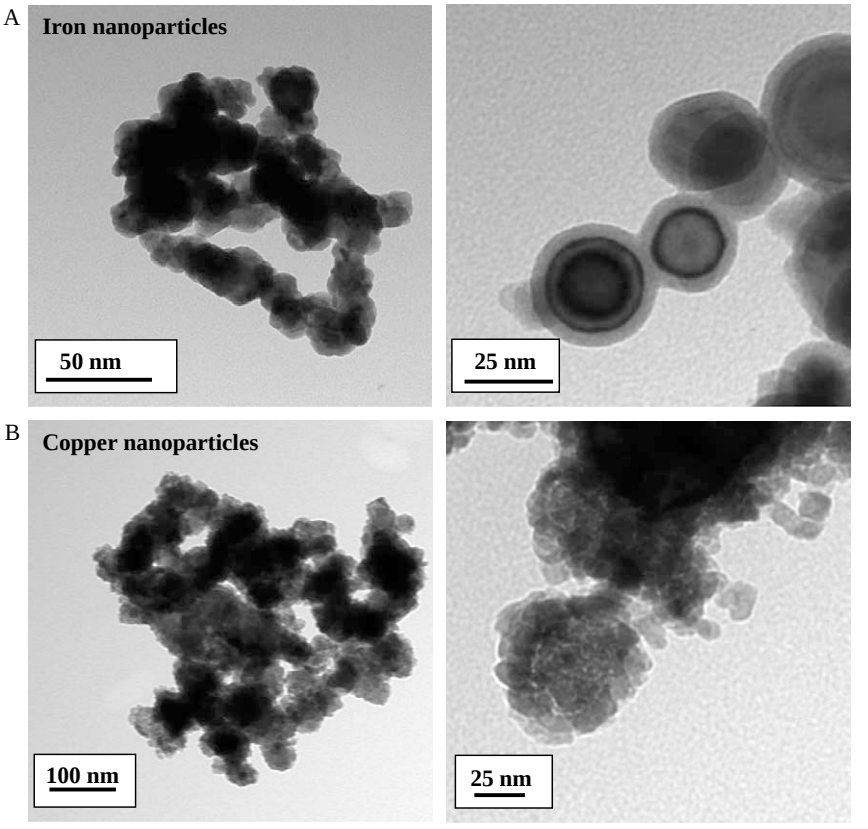

Figure 2. (A) TEM images of iron nanoparticle agglomerates generated in the exposure and collected in the whole-body inhalation chamber are shown. On the left, is a representative agglomerate formed in the chamber consisting of interlinking chains of particles. The TEM image on the right is a magnified view of a few single iron nanooparticles in an agglomerate. The isolated nanoparticles appear to show an iron core surrounded by an oxide coating. (B) TEM images of the copper nanoparticle agglomerates generated during exposure and collected in the whole-body inhalation chamber. The TEM on the left is a representative agglomerate formed in the chamber. The magnified view of the agglomerate is shown on the right. It can be seen that smaller particles form a dense agglomerate and that the primary particle size for the copper nanoparticles is around 12 nm. See text for futher details.

both iron and copper nanoparticles completely dissolved (see Figure 4) and the complete dissolution occurred in less than 3 h. Figure 4 shows the percentage of dissolved metal that was in solution after reaction from the original solid concentration added.

Because there are oxides layers present on both nanoparticles, the amounts of total iron and copper in the nanoparticles were determined by totally dissolving the metals in 1 M HCl solutions and the average of $n \geq 3$, was used as the amount of metal per weight of nanoparticles to determine total metal content of the nanoparticle suspension. For the iron nanoparticles, $80 \pm 2\%$ by weight was found to be elemental iron and for copper nanoparticles this was $92 \pm 3\%$ by weight. In acidic solutions, where pH was held relatively constant between 4.5–5.0 with the addition of HCl, there were very small amounts of soluble metal detected in solution after 24 h at 38°C for both iron and copper nanoparticles suggesting that the dissolving ions from the ALF solution were due to presence of the citric acid (Gorantla et al. 2005). This mechanism was further examined in a citric acid solution containing equal parts citric acid and sodium chloride adjusted to pH 4.5 with NaOH as in the ALF recipe. This citric acid solution also showed complete dissolution of both the copper and iron nanoparticles. Furthermore, there were also color changes of the solution seen as the nanoparticles dissolve in the ALF solution. Copper and iron ions were visibly bright blue and yellow, respectively, in ALF solutions.

In the Gamble's solution, representing airway surface liquid, there was a distinct difference in the amount of dissolved ions between iron and copper (Figure 4). The iron nanoparticles did not dissolve in the Gamble's solution after 24 h. In contrast, there was a measurable amount of dissolved copper in the Gamble's solution present at approximately 2% of the initial amount added to the reactor. Kinetic measurements showed that all copper dissolved in the first 60–70 min of the reaction after which no further dissolution occurred. Table II provides a summary of the physicochemical data

Table II. Summary of physiochemical characterization data of iron and copper nanoparticle aerosols.

	Iron nanoparticles	Copper nanoparticles
Primary particle size	25 ± 2 nm	12 ± 1 nm
Crystalline or amorphous material	Crystalline	Crystalline
Crystalline phases	Fe, Fe_3O_4, γ-Fe_2O_3	Cu, Cu_2O, CuO
Surface phase	γ-Fe_2O_3	CuO
Surface functionality	O, O-H and H_2O	O, O-H and H_2O
Surface area		
BET S.A.	17 ± 1 m^2 g^{-1}	12 ± 0.2 m^2 g^{-1}
Geometric S.A.*	ca. 35 m^2 g^{-1}	ca. 60 m^2 g^{-1}
Nanoparticle dissolution**	pH 7.2 $\ll$1%	pH 7.2 $\sim$1.1%
	pH 4.5 $\sim$100%	pH 4.5 $\sim$100%
Aerosol size distribution***		
Acute exposure	187.0 (1.3)	187.9 (1.3)
Sub-acute exposure	199.9 (1.3)	190.1 (1.3)

Surface area (S.A.); *Calculated from bulk weighted average densities of metal and metal oxides; **Nanoparticle dissolution measured at 38°C unless otherwise noted; ***GM, nm, (GSD) in exposure chamber.

for the nanoparticles including the dissolution studies results.

Acute exposure

Total and differential cell counts recovered from BAL fluid in animals exposed acutely to iron or copper nanoparticles were not significantly different than sentinel mice (Figure 5). However, the concentration of total protein was significantly ($p<0.01$) increased in animals exposed to copper in comparison to sentinels or iron exposed animals (Table III). We did not find significant changes in activity of LDH in BAL fluid of particle-exposed animals compared to controls. Total amounts of iron and copper in lung tissues in acutely exposed animals were measured by ICP/MS. The amount of iron measured in lungs of iron-exposed animals after subtracting the amount of iron found in sentinels, was 50 mg/kg lung (wet weight). When we subtracted the amount of copper found in sentinels from the average total of copper in copper nanoparticle-exposed mice, the value was 16.1 mg/kg lung (wet weight). According to our calculations, assuming a minute volume of 36 ml and particle deposition of 0.2, we estimated that the mass of particles delivered to the lungs to be 118 mg/kg lung (wet weight) of iron particles and 100 mg/kg lung (wet weight) of copper particle.

Sub-acute exposure

Neutrophilia were observed in animals exposed subacutely to iron or copper particles and necropsied at 0 wk post exposure (4.1% and 51.2%, respectively). The total number of cells as well as number of macrophages and lymphocytes in BAL fluid was also increased in these two groups of animals compared to sentinels; however, this increase was more predominant in animals exposed to copper than in the iron-exposed group (Table III and Figure 5).

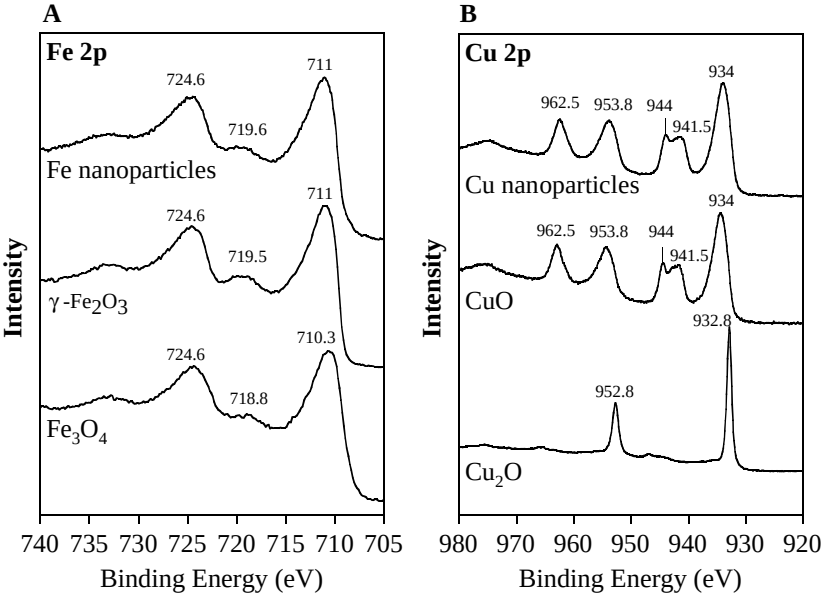

Figure 3. (A) XPS in the Fe 2p region is shown for iron nanoparticles along with reference spectra for Fe_3O_4 and γ-Fe_2O_3. Based on the similarities in peak position for all the peaks, the surface phase appears to be γ-Fe_2O_3. (B) XPS in the Cu 2p region is shown for copper nanoparticles along with reference spectra for of CuO and Cu_2O. The copper nanoparticles and CuO spectra are nearly identical and differ from the Cu_2O spectrum.

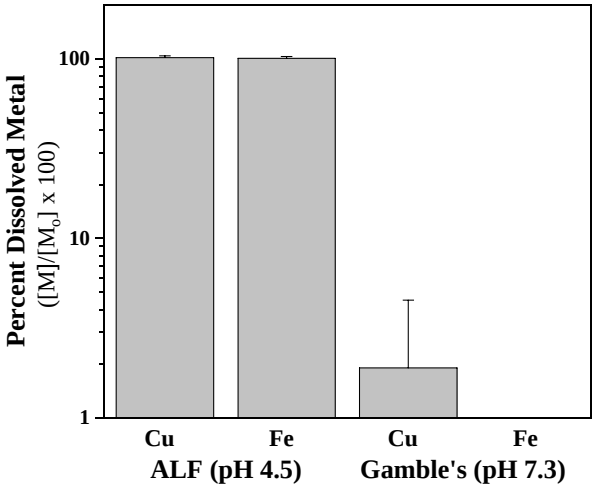

Figure 4. Summary of the dissolution experiments conducted in Gamble's and ALF solution for copper and iron nanoparticles. The data are shown as the percent metal dissolved, $M/M_o \times 100$, where M is the amount dissolved in 24 hours at 38°C and M_o is the total metal content of the nanoparticles. The amount of dissolved iron in the Gamble's solution was below the limit of detection. The error bars represent triplicate measurements.

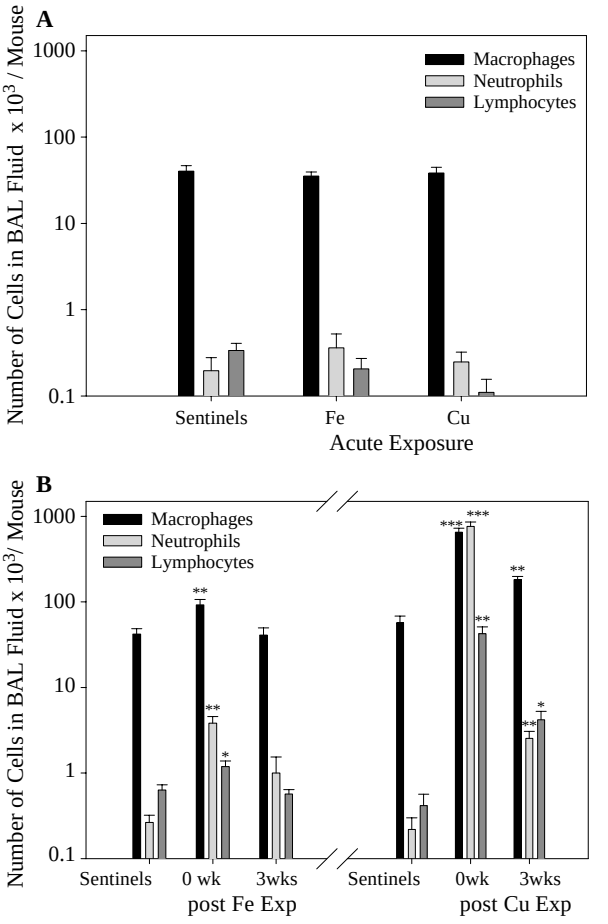

Figure 5. Number of cells in BAL fluid from animals acutely (A) and sub-acutely (B) exposed to iron and copper nanoparticles.

At 3 weeks post exposure, lung cells returned to baseline values for iron nanoparticle-exposed mice, but were still significantly increased for copper nanoparticle-exposed animals. Total protein levels and activity of LDH in BAL fluid were not significantly different for iron-exposed animals compared to sentinels. However, protein and LDH were significantly increased in mice exposed to copper nanoparticles and necropsied 0 wk post exposure. The concentration of total protein was nine times higher than sentinels and activity of LDH was 5.5 times higher than sentinels. At 3 weeks post exposure, these outcome variables had returned to baseline values in the copper-exposed mice.

Concentrations of the following cytokines/chemokines in BAL fluid in sentinels and in iron-exposed animals necropsied 0 or 3 weeks post exposure were below the lower limit of detection (LLOD, pg ml^{-1}): IL-3 (0.3), IL-4 (0.2), IL-5 (0.3), IL-10 (3.0), IL-12(p70) (0.2), INF-γ (0.1), MCP-1 (3.4), IL-17 (0.1), MIP-1α (2.0) and Eotaxin (43.9). The cytokine concentrations for iron-exposed animals are shown in Figure 6. In comparison with sentinels, KC ($p < 0.01$), TNF-α ($p < 0.02$) and G-CSF ($p < 0.05$) levels were significantly increased in the group necropsied immediately post exposure. At 3 weeks post exposure, TNF-α ($p < 0.05$), IL-2 ($p < 0.05$) and IL-13 ($p < 0.05$) remained significantly higher than sentinels, however these elevations were of limited biological significance. In copper nanoparticle-exposed animals necropsied at 0 wk post exposure, all cytokine/chemokine concentrations in BAL fluid that we measured were significantly increased except IL-2, IL-9 and IL-13 ($p < 0.001$: IL-1α, IL-5, IL-12p40, GM-CSF, KC, MCP-1, MIP-1β, RANTES, IL-1β, TNF-α, IL-6, IL-17, G-CSF, MIP-1α; $p < 0.01$: IL-3, IL-4, IL-10, IL-12p70, INF-γ and $p < 0.05$ for Eotaxin). After 3 weeks post exposure, all cytokine/chemokine concentrations had returned to baseline values (Figure 7).

Histopathology evaluation of the lungs from animals exposed to iron showed no signs of pathology. Micrographs of lung sections from exposed and sentinel animals are shown in Figure 8. In copper-exposed animals euthanized at 0 wk post exposure, we found perivasculitis and alveolitis (Figure 8A, 8B). Perivasculitis with minimal increase of inflammation and chronic inflammatory cells (score 1b) was found in all animals in this group. Alveolitis with minimal increase of inflammation and acute inflammatory cells (score 1a) was revealed in 88% (7 out of 8) animals in this group. There were no signs of fibrosis, peribronchiolitis or interstitial pneumonitis in any animals exposed to either nanoparticles or sentinels. Lung tissues from copper-exposed mice

Table III. Total protein and activity of LDH in BAL fluid for acute and sub-acute exposures.

Animal group	Total number of cells/mouse $\times 10^3 \pm$SE	Total protein, μg/ml ± SE	LDH activity, U/L ± SE
Acute exposure			
Sentinels	40.8 ± 6.5	76 ± 6	22 ± 7
Iron	36.0 ± 4.0	68 ± 3	16 ± 1
Copper	38.7 ± 6.3	156 ± 19**	24 ± 4
Sub-acute exposure			
Iron			
Sentinels	43.0 ± 6.7	171 ± 9	64 ± 5
0 wk	97.3 ± 15.5**	144 ± 20	50 ± 11
3 wks	42.5 ± 8.9	141 ± 8	30 ± 4
Copper			
Sentinels	57.6 ± 11.3	103 ± 9	31 ± 4
0 wk	1460.0 ± 153.0***	959 ± 138**	177 ± 32**
3 wks	188.8 ± 17.2***	100 ± 4	29 ± 3

Values are expressed as mean and standard error; *$p < 0.05$, **$p < 0.01$, ***$p < 0.001$ significantly different from sentinels.

necropsied 3 weeks post exposure (Figure 8C, 8D) and from sentinel mice (Figure 8E, 8F) were evaluated as normal.

Figure 9 shows the distribution of iron and copper nanoparticles in stained lung tissues. Our positive controls showed deep blue-stained nanoparticles for iron (Figure 9E) and brick red-stained nanoparticles for copper (Figure 9F) with dry particles using the Perls Prussian Blue Stain or Rhodanine Stain, respectively. We located free iron nanoparticles especially in the lung tissues harvested from animals necropsied immediately post exposure as well as engulfed in macrophages (Figure 9A). In lung tissues harvested from animals 3 weeks post exposure, the majority of iron nanoparticles were found inside the macrophages (Figure 9B). In copper exposed lungs,

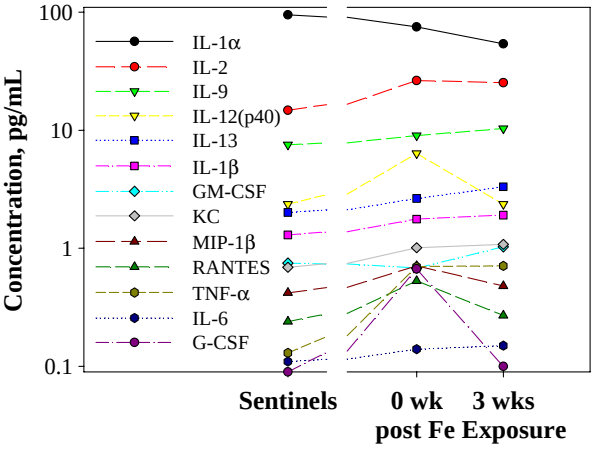

Figure 6. Cytokine/chemokine concentrations in BAL fluid in animals sub-acutely exposed to iron nanoparticles. The concentrations of following cytokines/chemokines in BAL fluid were bellow lowest limit of detection (LLOD): IL-3, IL-4, IL-5, IL-10, IL-12(p70), INF-γ, MCP-1, IL-17, MIP-1α and Eotaxin. In comparison with sentinels KC, TNF-α and G-CSF levels were significantly increased in group necropsied immediately post exposure. Data from sentinels were considered as baseline data.

there was no visual evidence of the presence of free nanoparticles or engulfed in macrophages at 0 or 3 weeks post exposure (Figure 9C, 9D).

Discussion

The purpose of the current study was to characterize pulmonary responses to inhaled iron or copper nanoparticles in healthy mice and compare their toxicity. We tested this using acute and sub-acute inhalation exposure models. These two different transition metal nanoparticles were fully characterized using bulk and surface methods. Although both nanoparticles were reported by the manufacturer to have average particle sizes of 25 nm, the copper nanoparticles were found to be approximately half the reported value but had a very narrow distribution. The iron nanoparticles were measured to be 25 ± 2 nm (Table II). Despite these differences in nanoparticle primary size, nanoparticle agglomerates were of comparable size with geometric mean mobility diameters between 187 and 200 nm (Table II).

Both metal nanoparticles were passivated with oxygen in the manufacturing process and XRD patterns of the iron and copper nanoparticles showed the presence of three distinct phases. XPS data provided spectral evidence for an outermost surface coating of the most oxidized phase, γ-Fe_2O_3 and CuO, for iron and copper nanoparticles, respectively. Both nanoparticles have a concentration gradient of oxidation from a core of reduced metal to a layer of a partially oxidized phase to a surface layer of a completely oxidized phase. It is important to understand the structural make up of the particles because the surface-cellular interactions will play a key role in the biological response and chemical properties, e.g., the solubility will depend on surface composition and surface reactivity.

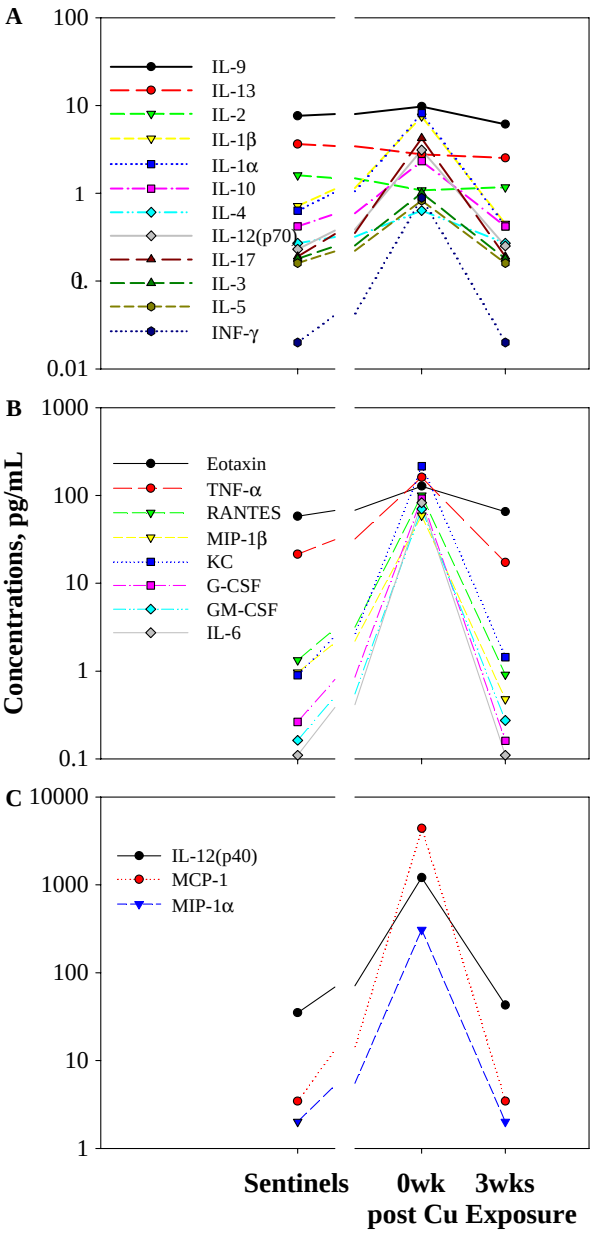

Figure 7. (A, B, C) Cytokine/chemokine concentrations in BAL fluid in animals sub-acutely exposed to copper particles. In comparison with sentinels, all concentrations except IL-2, IL-9 and IL-13 were significantly increased in animals necropsied at 0 week post exposure.

The results of our murine exposures show the copper nanoparticles to be significantly more toxic than iron nanoparticles. For the sub-acute exposure, there was a greater inflammatory response for copper than iron nanoparticles in mice necropsied immediately after exposure as evidenced by higher numbers of macrophages and neutrophils, higher concentration of total protein, increased LDH activity (Figure 5), elevation of a large number of cytokines (Figures 6 and 7) and histopathological evidence (Figure 8). In the iron exposure, only a small number of neutrophils (200-fold less than copper) were present in the BAL fluid in mice necropsied immediately after exposure indicating the presence of less inflammation.

The pro-inflammatory cytokine TNF-α was significantly elevated only in BAL fluid recovered from copper-exposed lungs. As observed in a previous inhalation study in rats, exposure to carbon black particles may be responsible for monocyte/macrophages recruitment (Driscoll et al. 1996). Out of all cytokines measured, MCP-1 was elevated the most in the sub-acute copper nanoparticle-exposed group (from 3.4 in sentinels to 4398.1 pg/ml in group necropsied immediately post exposure). This increase was consistent with increased numbers of BAL macrophages. Other cytokines/chemokines that were highly elevated in copper nanoparticle-exposed animals were IL-12 (p40), MIP-1α, KC, Eotaxin and RANTES. Interestingly, we observed augmentation of IL-12 (p40) cytokine that is known to be elevated with pro-fibrogenic exposures (Shvedova et al. 2007). The levels increased from an average concentration of 35 pg/ml in controls to 1211 pg/ml in animals exposed to copper nanoparticles, however we did not find fibrotic changes in lung tissues in animals necropsied immediately or 3 weeks post exposure (Figure 8).

Furthermore, in the iron nanoparticle exposure all parameters measured in BAL fluid of lungs returned to baseline values 3 weeks post exposure. This was not true for copper nanoparticle-exposed animals. Though the number of inflammatory cells decreased, they were still significantly elevated 3 weeks post exposure compared to controls. All other parameters including lung tissue pathology returned to normal values for both the iron and copper nanoparticle-exposed mice. Perivasculitis and alveolitis (inflammatory cells, primarily lymphocytes, surrounding a blood vessel and a bronchiole) were found in lung tissue of copper nanoparticle-exposed animals. However, there was no evidence for peribronchiolitis as is commonly seen with exposure to pro-inflammatory particulate matter. The absence might be an indication of particle translocation to the blood.

The acute exposure study was conducted to determine if the induction of inflammatory responses required multiple exposures. Acute 4-h-exposure to either iron or copper nanoparticles at twice the daily exposure levels used in the subacute study produced no significant changes with the exception of total protein concentration in copper nanoparticle-exposed animals. The low inflammatory response in the acute study suggests that repeated exposures were needed to achieve a sufficient lung burden or to overwhelm clearance and repair mechanisms.

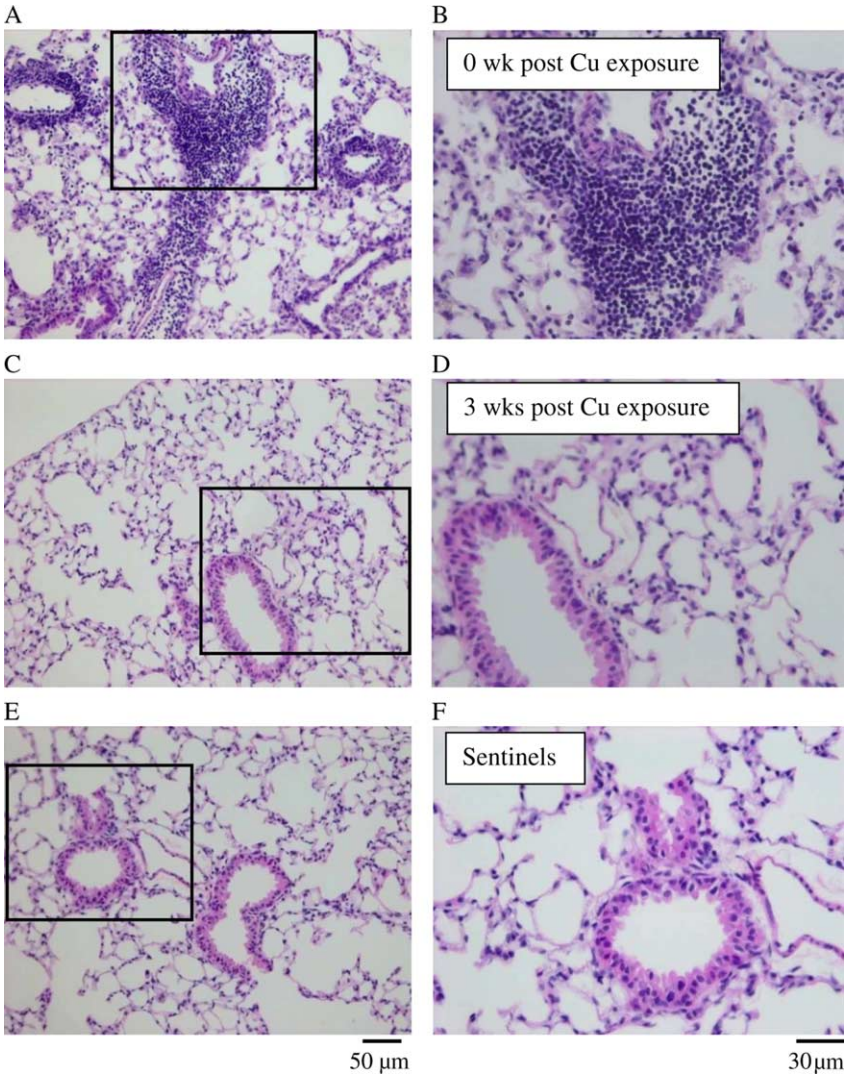

Figure 8. Micrographs of lung sections stained with H&E from mice sub-acutely exposed to copper nanoparticles and necropsied immediately after the last exposure (A, B), mice exposed to copper particles and necropsied 3 weeks post exposure (C, D) and sentinels (E, F). The areas indicated by the box in the low magnification figures are shown at higher magnification in the micrographs.

The physical and chemical properties of the nanoparticles can also change following deposition into the lungs. Metal nanoparticle properties may change due to the presence of phagocytes, different pH environments or through interaction with cellular components. Dissolution of the nanoparticles and the concomitant change in nanoparticle size, once inhaled, could lead to time dependent changes in the inflammatory response. The copper, but not the iron, nanoparticles were shown to partially dissolve in the Gamble's solution, whereas no detectable iron was measured in the same solution. Although copper is an essential trace element, excess copper intake has been shown to be toxic (Chen et al. 2006) and induce pulmonary inflammation characterized by increased neutrophils (Rice et al. 2001). The results reported here are consistent with previous studies of copper materials in artificial and biological media, e.g., saliva, lung fluid or blood, which had a propensity to dissolve (Chen et al. 2006; Midander et al. 2007). Furthermore, it was also shown that the initial rate of dissolution of copper and copper oxides was higher for materials with higher surface areas compared to sheeted copper patina in almost all solutions (pH ranging from 4.5–7.4) (Midander et al. 2007) as well as in *in vitro* and *in vivo* studies (Meng et al. 2007).

Iron exposure studies in rats suggest that addition of soluble transition metals (iron salts) to ultrafine particles (carbon black) can enhance production of inflammation (Wilson et al. 2002). The enhancement or singular cause of inflammatory response in transition metals has been shown to be proportional to the solubility of the metal in the biological

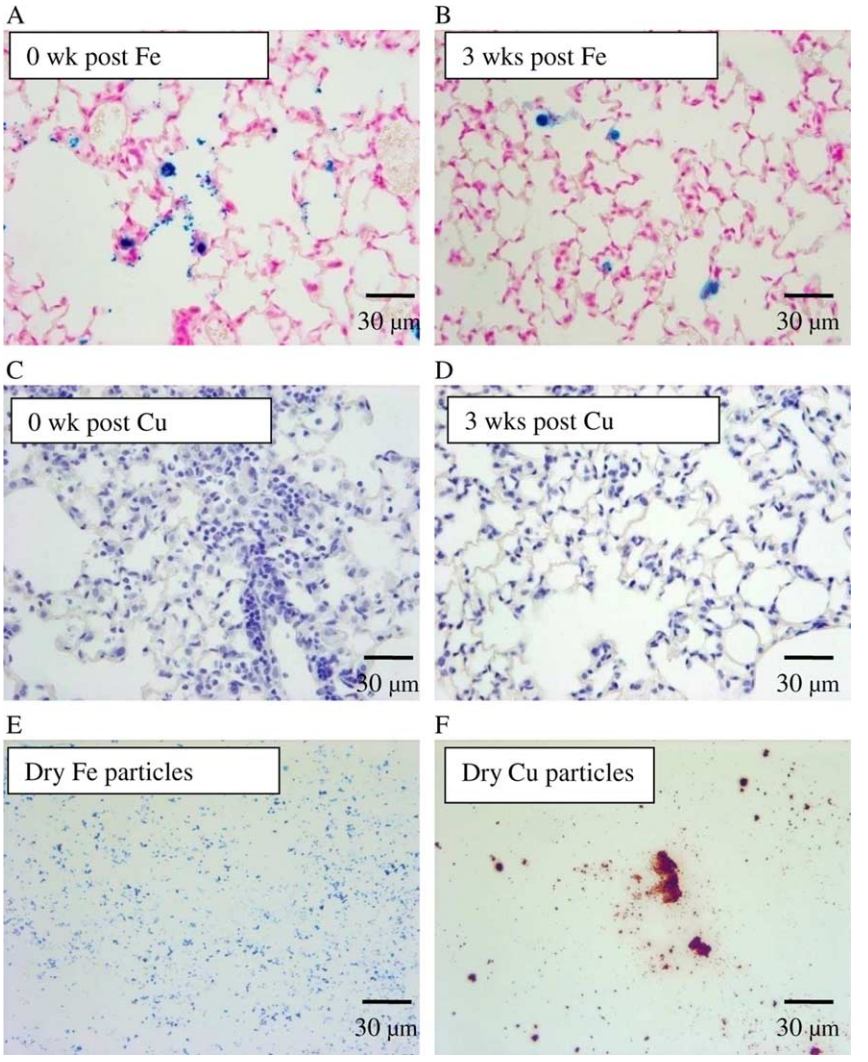

Figure 9. Lung tissues were stained to illuminate iron (deep blue) and copper (brick red) nanoparticles. The distributions of iron and copper stained nanoparticles in lung tissues (A, B, C, D), as dry powder (E, F) are shown. Iron nanoparticles were visible in lung sections at both 0 and 3 weeks post exposure (A, B), but copper nanoparticles were not visible in the lung tissue (C, D). Nanoparticles deposited on the slide as dry powder (E, F) were used as positive controls.

media (Knaapen et al. 2002; Borm et al. 2006; Brunner et al. 2006; Midander et al. 2007). Although both soluble and insoluble metal nanoparticles produce inflammatory responses, the pathways for inflammation differ. Exposures of copper nanoparticles and soluble copper salts to zebrafish showed there were differences in the biological responses that could not be explained simply by amount of dissolution (Griffitt et al. 2007). Exposure studies using fully oxidized iron nanoparticles, γ-Fe_2O_3, demonstrated dose-dependent inflammatory responses with sizes ranging from 20–140 nm at a dose of 57 and 90 $\mu g/m^3$ (Zhou et al. 2003). Fe_2O_3 particles 5–12 nm in diameter suppressed PC12 cell function during *in vitro* studies also in a dose dependent trend (Pisanic et al. 2007), but large inflammatory responses were not observed in the current inhalation studies.

In the studies reported herein, iron nanoparticles did not dissolve in Gamble's solution up to 48 h. Although the iron nanoparticles did completely dissolve in the ALF fluid, there were accumulated nanoparticles in the macrophages shown in Figure 9. Alveolar macrophages are key cells in initiating inflammation and oxidative stress responses. Previous studies have shown that iron oxide particles had very low solubility, were less capable of producing reactive oxygen species (ROS), and did not cause inflammatory responses after intra-tracheal instillation to rats (Lay et al. 1999). Because iron metal would have a greater propensity to dissolve in the interstitial and phagolysomal fluids than iron oxide and enhance inflammatory response as seen in previous studies, this indicates that the inflammatory response of the iron nanoparticles in our study may

be more a function of the outer oxidized layer rather than the iron core. Reduced iron would more readily dissolve in the Gamble's fluid creating more soluble ions in solution. The enhanced effect of soluble metal may activate the macrophages increasing the inflammatory response as was seen in previous studies. Furthermore, the low biological response is consistent with other magnetic nanoparticle studies that were conducted on different compositions being used in medicinal applications that were found to be nontoxic (Kim et al. 2006).

As mentioned previously, the relatively high concentrations of copper nanoparticles did not show a large inflammatory response in the acute studies and the clearance could have been sufficient not to overburden the lungs. Interestingly for the sub-acute exposures, the copper nanoparticles were never seen in lung histopathology accumulating in macrophages at zero or three weeks post exposure while the iron nanoparticles were clearly visible at both time points (Figure 9). The absence of peribronchiolitis along with no accumulation suggests the possibility of translocation out of the pulmonary system to other organs. Translocation of copper nanoparticles has been reported by Chen et al. (2006). They showed the main target organs were the kidney, liver and spleen when mice were exposed to 23 nm copper particles. In addition, these organs showed significant change in color and size in exposed mice. The nanoparticles also could have been well dispersed in the interstitial spaces creating small agglomerates, too small to be seen with the optical microscope.

Copper particles have been reported to produce oxidative stress in the cells through hydroxyl radical and hydrogen peroxide production (Valko et al. 2005). Oxidative stress may not be the only mechanistic pathway to cellular toxicity for iron and copper. It has been suggested that transition metals induce pulmonary inflammation by different pathways or combination of signals, as it was shown in rat instillation exposures to metal sulfates (Rice et al. 2001). Monitoring the different cytokine levels in exposure studies can give valuable information on the type of injury or response occurring because specific cytokines partially control inflammatory processes by recruiting inflammatory cells to the lungs after exposure to foreign particles (Driscoll et al. 1997). In the studies conducted by Rice et al. (2001) copper sulfate salt was shown to be the most proinflammatory (high neutrophilia) and cytotoxic metal from all other metal sulfates studied (vanadium, nickel, iron(II), manganese and zinc).

Data from previous studies indicates that size and the amount of soluble ions in solution increase the inflammatory response. Thus, it is reasonable to hypothesize that smaller nanoparticles with greater surface area will have a larger propensity of metal dissolution resulting in an increased inflammatory response. Because copper nanoparticles were not found in stained lung micrographs in macrophages or in the interstitial spaces, the increased response may be a combination of translocation and soluble metal ion activity. As the copper nanoparticles undergo dissolution, they will yield dissolved ions and concomitantly decrease in size below 10 nm in diameter based on the extent of dissolution. It is important to recognize change in size may alter the physicochemical properties of the nanoparticles requiring further considerations. For example, there will be changes in the electronic properties of the nanoparticles, as suggested by the change in the copper nanoparticle color during dissolution, as the nanoparticles change size. Therefore, the interaction with the biological media will change as the nanoparticles become smaller and could deagglomerate in a more acidic environment. Changes in surface reactivity will affect nanoparticle-cellular interactions. Ultimately, further studies using state-of-the-art imaging techniques that can follow nanoparticles *in vivo* are needed to address these possibilities.

Conclusion

The sub-acute and acute exposure studies conducted were designed to examine the inflammatory response of two transition metal nanoparticles in mice, copper and iron. Copper nanoparticles induced a greater inflammatory response based on neutrophilia, macrophages and total cell count from the BAL fluid as well as an increase in almost all cytokine levels measured when compared to the iron nanoparticles in the sub-acute studies. Histopathology of the lungs 0 and 3 weeks post exposure showed no presence of copper where as iron was found accumulating in macrophages. *In vitro* dissolution studies showed a greater propensity of copper to dissolve in the biological fluid increasing ion concentration and concomitantly decreasing the size of the nanoparticles. The increased inflammatory response of copper in the mouse model is proposed to be associated with the nanoparticle size and increased ion concentration produced from the dissolving nanoparticles *in vivo*.

Acknowledgements

Although the research described in this article has been funded wholly or in part by the Environmental Protection Agency through grant number EPA RD-83171701-0 to VHG, PTO and PST, it has not been subjected to the Agency's required peer and policy

review and therefore does not necessarily reflect the views of the Agency and no official endorsement should be inferred. NIOSH support is also acknowledged through R01 OH009448-01. NIEHS supported the Pulmonary Toxicology Facility through NIH P30 ES05605. Competing financial interest statement: Vicki H. Grassian is paid a consulting fee as a member of the science advisory board of Northern Nanotech Inc. Toronto, Canada, and Nanoscale Materials Inc. of Manhattan, Kansas, and owns stock shares in that company. All of the other authors declare they have no competing financial interests.

***Declaration of interest*:** The authors report no conflicts of interest. The authors alone are responsible for the content and writing of the paper.

References

Al-Abadleh HA, Grassian VH. 2003. Oxide surfaces as environmental interfaces. Surf Sci Rep 52:63–161.

Anjilvel S, Asgharian B. 1995. A multiple-path model of particle deposition in the rat lung. Fundam Appl Toxicol 28:41–50.

ASTM International Committee E56 on Nanotechnology, ASTM E2456-06 Standard Terminology for Nanotechnology is available at www.astm.org.

Atkins P, de Paula J. 2002. Physical Chemistry, 7th ed.; W.H. Freeman and Company: New York.

Babes L, Denizot B, Tanguy G, Le Jeune JJ, Jallet P. 1999. Synthesis of iron oxide nanoparticles used as MRI contrast agents: A parametric study. J Colloid Interface Sci 212: 474–482

Balbus J, Maynard AD, Colvin VL, Castranova V, Daston GP, Denison RA, Dreher KL, Goering PL, Goldberg AM, Kulinowski KM, Monteiro-Riviere NA, Oberdörster G, Omenn GS, Pinkerton KE, Ramos KS, Rest KM, Sass JB, Silbergeld EK, Wong BA. 2007. Hazard assessment for nanoparticles – report from an interdisciplinary workshop. Environ Health Perspect 115:1654–1659.

Borm P, Klaessig FC, Landry TD, Moudgil B, Pauluhn J, Thomas K, Trottier R, Wood S. 2006. Research strategies for safety evaluation of nanomaterials. Part V: Role of dissolution in biological fate and effects of nanoscale particles. Toxicol Sci 90:23–32.

Brunner TJ, Wick P, Manser P, Spohn P, Grass RN, Limbach LK, Bruinink A, Stark WJ. 2006. *In vitro* cytotoxicity of oxide nanoparticles: Comparison to asbestos, silica, and the effect of particle solubility. Environ Sci Technol 40:4374–4381.

Chen Z, Meng H, Xing G, Chen C, Zhao Y, Jia G, Wang T, Yuan H, Ye C, Zhao F, Chai Z, Zhu C, Fang X, Ma B, Wan L. 2006. Acute toxicological effects of copper nanoparticles *in vivo*. Toxicol Lett 163:109–120.

Chen D, Gao L. 2004. A facile route for high-throughput formation of single-crystal alpha-Fe_2O_3 nanodisks in aqueous solutions of Tween 80 and triblock copolymer. Chem Phys Lett 395:316–320.

Downs RT, Hall-Wallace M. 2003. The American Mineralogist Crystal Structure Database. Am Mineralogist 88:247–250.

Driscoll KE, Carter JM, Hassenbein DG, Howard B. 1997. Cytokines and particle-induced inflammatory cell recruitment. Environ Health Perspect 105(Suppl. 5):1159–1164.

Driscoll KE, Carter JM, Howard BW, Hassenbein DG, Pepelko W, Baggs RB, et al. 1996. Pulmonary inflammatory, chemokine, and mutagenic responses in rats after subchronic inhalation of carbon black. Toxicol Appl Pharm 136:372–380.

Driscoll KE, Costa DL, Hatch G, Henderson R, Oberdörster G, Salem H, Schlesinger RB. 2000. Intratracheal instillation as an exposure technique for the evaluation of respiratory tract toxicity: uses and limitations. Toxicol Sci 55:24–35.

Gilbert B, Huang F, Zhang H, Waychunas GA, Banfield JF. 2004. Nanoparticles: Strained and stiff. Science 305:651–654.

Gorantla VRK, Assiongbon KA, Babu SV, Roy D. 2005. Citric acid as a complexing agent in CMP of copper: Investigation of surface reactions using impedance spectroscopy. J Electrochem Soc 152:G404–410.

Grassian VH, O'Shaughnessy P T, Adamcakova-Dodd A, Pettibone JM, Thorne PS. 2007a. Inhalation exposure study of titanium dioxide nanoparticles with a primary particle size of 2 to 5 nm. Environ Health Perspect 115:397–402.

Grassian VH, O'Shaughnessy PT, Adamcakova-Dodd A, Pettibone JM, Thorne PS. 2007b. Nanotoxicology 1:211–226.

Griffitt RJ, Weil R, Hyndman KA, Denslow ND, Powers K, Taylor D, Barber DS. 2007. Exposure to copper nanoparticles causes gill injury and acute lethality in zebrafish (danio rerio). Environ Sci Technol 41:8178–8186.

Hamelin ME, Prince GA, Gomez AM, Kinkead R, Boivin G. 2006. Human metapneumovirus infection induces long-term pulmonary inflammation associated with airway obstruction and hyperresponsiveness in mice. J Infect Dis 193:1634–1642.

Hsieh TH, Yu CP, Oberdörster G. 1999. Deposition and clearance models of Ni compounds in the mouse lung and comparisons with the rat models. Aerosol Sci Technol 31: 358–372.

Kakkar R, Kapoor PN, Klabunde KJ. 2004. Theoretical study of the adsorption of formaldehyde on magnesium oxide nanosurfaces: Size effects and the role of low-coordinated and defect sites. J Phys Chem C 108:18140–18148.

Kim JS, Yoon T, Yu KN, Kim BG, Park SJ, Kim HW, Lee KH, Park SB, Lee J, Cho MH. 2006. Toxicity and tissue distribution of magnetic nanoparticles in mice. Toxicol Sci 89:338–347.

Knaapen AM, Shi T, Borm PJA, Schins RPF. 2002. Soluble metals as well as the insoluble particle fraction are involved in cellular DNA damage induce by particulate matter. Mol Cell Biochem 234/235:317–326.

Lai YL. 1991. Comparative ventilation of the normal lung. In: Parent RA, editor. Comparative biology of the normal lung. Boca Raton, FL: CRC Press. pp 217–240.

Lay JC, Bennett WD, Ghio AJ, Bromberg PA, Costa DL, Kim CS, et al. 1999. Cellular and biochemical response of the human lung after intrapulmonary instillation of ferric oxide particles. Am J Respir Cell Mol Biol 20:631–642.

Liu G, Li1 X, Qin B, Xing D, Guo Y, Fan R. 2004. Investigation of the mending effect and mechanism of copper nano-particles on a tribologically stressed surface. Tribol Lett 17:961–966.

Meng H, Chen Z, Xing G, Yuan H, Chen C, Zhao F, Zhang C, Wang Y, Zhao Y. 2007. Ultra high reactivity and grave nanotoxicity of copper nanoparticles. J Radioanal Nucl Chem 272:595–598.

Midander K, Pan J, Leygraf C. 2006. Elaboration of a test method for the study of metal release from stainless steel particles in artificial biological media. Corrosion Sci 48:2855–2866.

Midander K, Wallinder IO, Leygraf C. 2007. *In vitro* studies of copper release from powder particles in synthetic biological media. Environ Pollut 145:51–59.

Moss OR. 1979. Simulants of lung interstitial fluid. Health Phys 36:447–448.

Moss OR, Wong VA. 2007. When nanoparticles get in the way: Impact of projected area on *in vivo* and *in vitro* macrophage function. Inhal Toxicol 18:711–716.

Oberdörster G, Oberdörster E, Oberdörster J. 2005. Nanotoxicology: An emerging discipline evolving from studies. Environ Health Perspect 113:823–839.

O'Shaughnessy PT, Achutan C, O'Neill ME, Thorne PS. 2003. A small whole-body exposure chamber for laboratory use. Inha Toxicol 15:251–263.

Osier M, Oberdörster G. 1997. Intratracheal inhalation vs. intratracheal instillation: Differences in particle effects. Fundam Appl Toxicol 40:220–227.

Pisanic TR II, Blackwell JD, Shubayev VI, Finones RR, Jin S. 2007. Nanotoxicity of iron oxide nanoparticle internalization in growing neurons. Biomaterials 28:2572–2581.

Powers KW, Palazuelos M, Moudgil BJ, Roberts SM. 2007. Characterization of the size, shape, and state of dispersion of nanoparticles for toxicological studies. Nanotoxicology 1: 42–51.

Rice TM, Clarke RW, Godleski JJ, Al-Mutairi E, Jiang NF, Hauser R, Paulauskis JD. 2001. Differential ability of transition metals to induce pulmonary inflammation. Toxicol Appl Pharmacol 177:46–53.

Sayes CM, Reed KL, Warheit DB. 2007. Assessing toxicity of fine and nanoparticles: Comparing *in vitro* measurements to *in vivo* pulmonary toxicity profiles. Toxicol Sci 97:163–180.

Seagrave JC, McDonald JD, Mauderly JL. 2005. *In vitro* versus *in vivo* exposure to combustion emissions. Exp Toxicol Pathol 57:233–238.

Shvedova AA, Fabisiak JP, Kisin ER, Murray AR, Roberts JR, Tyurina YY, Antonini JM, Feng WH, Kommineni C, Reynolds J, Barchowsky A, Castranova V, Kagan VE. 2008. Sequential exposure to carbon nanotubes and bacteria enhances pulmonary inflammation and infectivity. Am J Respir Cell Mol Biol 38:579–590.

Stopford W, Turner J, Cappellini D, Brock T. 2003. Bioaccessibility testing of cobalt compounds. J Environ Monit 5:675–680.

Thorne PS, Adamcakova-Dodd A, Kelly KM, O'Neill ME, Duchaine C. 2006. Metalworking fluid with mycobacteria and endotoxin induces hypersensitivity pneumonitis in mice. Am J Respir Crit Care Med 173:759–768.

Valko M, Morris H, Cronin MT. 2005. Metals, toxicity and oxidative stress. Curr Med Chem 12:1161–1208.

Warheit DB, Borm PJA, Hennes C, Lademann J. 2007. Testing strategies to establish the safety of nanomaterials: Conclusions of an ECETOC workshop. Inhal Toxicol 19:631–643.

Wilson MR, Lightbody JH, Donaldson K, Sales J, Stone V. 2002. Interactions between ultrafine particles and transition metals in vivo and in vitro. Toxicol Appl Pharm 184:172–179.

Wu C, Yin M, O'Brien S, Koberstein JT. 2006. Quantitative analysis of copper oxide nanoparticle composition and structure by x-ray photoelectron spectroscopy. Chem Mater 18:6054–6058.

Yin M, Wu C, Lou Y, Burda C, Koberstein JT, Zhu Y, O'Brien S. 2005. Copper oxide nanocrystals. J Am Chem Soc 127: 9506–9511.

Zhang H, Penn RL, Hamers RJ, Banfield JF. 1999. Enhanced adsorption of molecules on surfaces of nanocrystalline particles. J Phys Chem B 103:4656–4662.

Zhang W. 2003. Nanoscale iron particles for environmental remediation: An overview. J Nanopart Res 5:323–332.

Zhou YM, Zhong CY, Kennedy IM, Pinkerton KE. 2003. Pulmonary responses of acute exposure to ultrafine iron particles in healthy adult rats. Environ Toxicol 18:227–235.

This paper was first published online on iFirst on 13 October 2008.